PHARMACIA

Pharmacia 71: 1–12
DOI 10.3897/pharmacia.71.e117192

Research Article

Docking, synthesis, and anticancer assessment of novel quinoline-amidrazone hybrids

Ahmad H. Abdullah[1], Ahmad K. Alarareh[1], Mahmoud A. Al-Sha'er[1], Almeqdad Y. Habashneh[2], Firas F. Awwadi[2], Sanaa K. Bardaweel[3]

1 *Faculty of Pharmacy, Zarqa University, Zarqa, 13132, Jordan*
2 *Faculty of Science, The University of Jordan, Amman, 11942, Jordan*
3 *School of Pharmacy, The University of Jordan, Amman, 11942, Jordan*

Corresponding author: Ahmad H. Abdullah (aabdullah@zu.edu.jo)

Received 11 December 2023 ♦ **Accepted** 26 December 2023 ♦ **Published** 15 January 2024

Citation: Abdullah AH, Alarareh AK, Al-Sha'er MA, Habashneh AY, Awwadi FF, Bardaweel SK (2024) Docking, synthesis, and anticancer assessment of novel quinoline-amidrazone hybrids. Pharmacia 71: 1–12. https://doi.org/10.3897/pharmacia.71.e117192

Abstract

A group of new amidrazone compounds that include a quinoline component was produced through the reaction of hydrazonyl chloride, derived from 6-aminoquinoline, with appropriate secondary cyclic amines. The new compounds were confirmed through ^{1}H-NMR, ^{13}C-NMR, FTIR, and HRMS, and further verified by single-crystal X-ray diffraction. The antitumor potential of the synthesized compounds was tested against lung cancer (A549) and breast cancer (MCF-7) cell lines. Among the compounds, the ethyl carboxylate and o-hydroxy phenyl piperazine derivatives (**10d** and **10g**) exhibited the strongest activity against both cell lines, with IC_{50} values of 43.1 and 59.1 μM for the lung and breast cancer cell lines, respectively. Moreover, the most potent compounds were subsequently docked into the c-Abl kinase binding site (PDB code: 1IEP) as a possible anticancer mechanism. *In-silico* ADMET study shows acceptable pharmacokinetic properties, and the toxicity profile for the most potent compounds is non-carcinogenic.

Keywords

Amidrazones, anti-tumor, c-Abl kinase, Japp-Klingmann reaction, (ADME)

Introduction

Quinoline derivatives have exhibited great potential as effective anticancer agents by selectively targeting and inhibiting the growth and proliferation of cancer cells (Ilakiyalakshmi and Napoleon 2022). Moreover, compounds containing a quinoline nucleus have demonstrated diverse biological activities, including antibacterial (Ranjbar-Karimi et al. 2018), antimalarial (Kalaria et al. 2018), and antiviral properties (Guardia et al. 2018). Naturally occurring quinoline alkaloids such as Cinchona (Sang-sup et al. 2009), and Dictamnine (Jain et al. 2019) have already been used to treat various types of cancer (Fig. 1). Additionally, several synthetic quinolines, such as Neratinin, Acridinecarboxamide, and Cabozantinib, have been approved by the U.S. Food and Drug Administration (FDA) for the treatment of different types of cancer (Fig. 2). On the other hand, numerous piperazine-incorporating amidrazones, including compounds **1–5** (Fig. 3), have been identified as potential anticancer scaffolds due to their ability to target specific enzymes and receptors involved in tumor growth (Paprocka et al. 2022). As such, the development of new anticancer drugs based on these scaffolds (piperazine, amidrazone, and quinoline) is an active area of research, with their capacity to target multiple pathways involved in cancer development making them attractive candidates for drug discovery. This paper provides a comprehensive account of the synthesis, spectroscopic characterization, and in-silico ADMET analysis

aimed at assessing the pharmacokinetic properties and toxicity profile of novel piperazinyl amidrazones that incorporate quinoline components. Additionally, it delves into their evaluation of antitumor activity. The proposed mechanism of action involves the inhibition of c-Abl kinase, as elucidated through docking techniques. Nevertheless, it is worth noting that further in vitro enzyme assays are planned for the future to validate this proposed mechanism (Paprocka et al. 2022). The synthetic compounds have been designed and synthesized with the intent of being selective and potential agents against cancer, with a primary focus on their role as c-Abl kinase inhibitors (Paprocka et al. 2022).

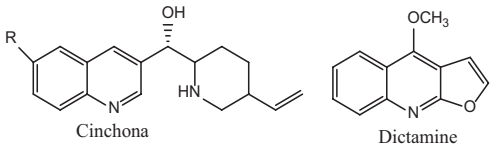

Figure 1. Structure representation of quinoline-based natural alkaloids.

Experimental part

Materials and method

The open capillary method on a Melting Point Meter M3000 (KRÜSS Optronic, Germany) was used to determine the melting points, which are uncorrected. The PerkinElmer Spectrum Two FT-IR Spectrometer (Diamond ATR FTIR) (Perkin-Elmer, USA) was employed to record the IR spectra, with a spectral resolution of 4 cm^{-1} and a range of 4000 – 400 cm^{-1}. Bruker Avance Spectrometer AV500 (Bruker, Germany) was used to record ^{1}H, ^{13}C NMR, and ^{2}D NMR spectra, with DMSO d_6 as the solvent and TMS as an internal standard; chemical shifts were expressed in δ units, and the J value was given in Hertz. HRMS measurements were conducted using the electrospray ion trap (ESI) technique by collision-induced dissociation on a Bruker APEX-4 (7 Tesla) instrument in positive or negative ion mode. The samples were dissolved in chloroform and infused using a syringe pump with a flow rate of 2 μL/min,

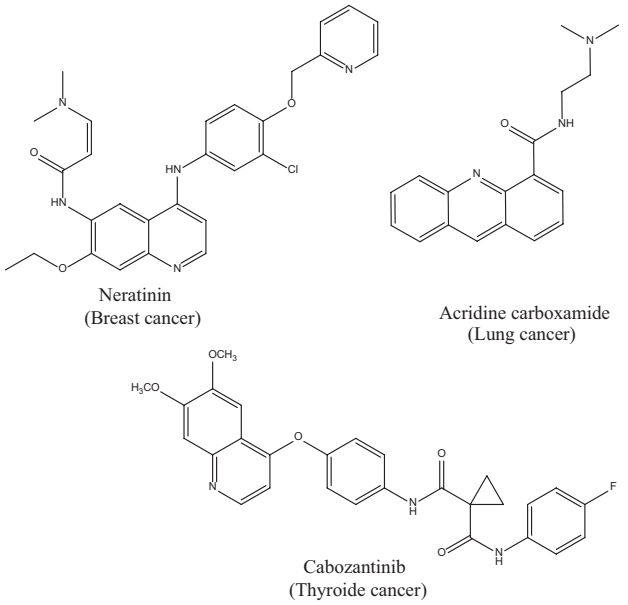

Figure 2. Anticancer drugs with their structures.

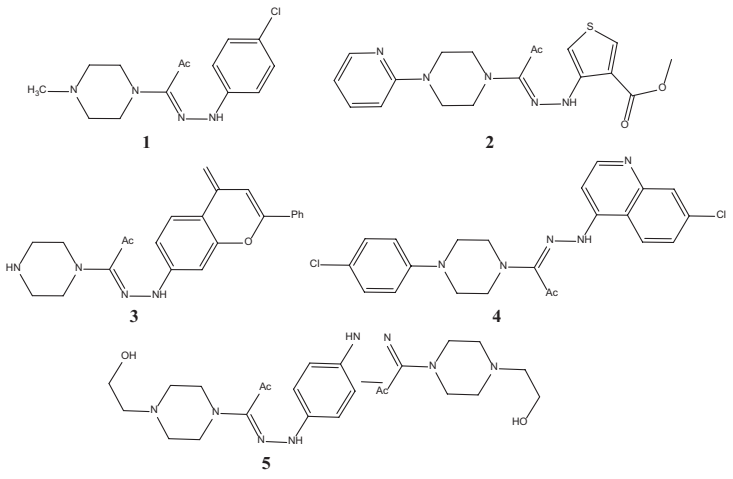

Figure 3. The Amidrazones structures of antitumor compounds **1–5.**

and external calibration was carried out using an arginine cluster in a mass range of m/z 175–871, with a mass error of 0.00–0.50 ppm. CrysAlisPro was utilized to determine and refine cell properties with multiscan absorption collection and transmission factors of 1.00000 and 0.00000 as maximum and minimum. The structure was solved using Direct Methods and refined using full-matrix least-squares on F2, with non-hydrogen atoms anisotropically refined, and hydrogen atoms placed in estimated locations and refined using a riding model. All reactions were monitored by thin layer chromatography, performed on silica gel 60 WF254S aluminum sheets (Merck, Germany), and visualized using UV light. Chemical reagents in high purity were purchased from Acros Organics (in Belgium). Software: Licensed Biovia 4.5 installed on the USER-THINK server with the following properties; CPU 3.1 GH, RAM 8.00 GB, System type 64 bit, Windows 7.

Chemistry

General procedure for the synthesis of *N*-(quinolin-6-yl)propanehydrazonoyl chloride (8)

The given compound was synthesized using the following steps: In step (i), a solution of Compound 6-aminoquinoline **6** (2.6 g, 0.01 mol) in 6N aqueous hydrochloric acid (16 mL) was prepared. Sodium nitrite (0.76 g, 0.011 mol) dissolved in water (1.5 mL) was added drop-wise to this solution with efficient stirring at 0–5 °C. The mixture was stirred for 20–30 min. In step (ii), the resulting quinolin-6-diazonium chloride **6A** solution, obtained from step (i), was added to a cold solution (0 to -10 °C, ice-salt bath) of 3-chloropentan-2,4-dione (1.35 g, 0.01 mol) in ethanol/water (16 mL, 1:1 v/v) containing 30.0 g of sodium acetate, with vigorous stirring. The mixture was stirred until a solid precipitate formed (5–10 min). The reaction mixture was then diluted with cold water (250 mL). The solid product was collected by suction filtration, washed several times with cold water, and dried. The resulting product was solid with a brownish color. Yield: 94%, brownish powder, mp 197 °C dec; R_f = 0.71: dichloromethane/methanol = 9.75:0.25 by volume). IR (KBr) n 1026, 1171, 1215, 1542, 1689, 2938, 3105 cm^{-1}; ^{1}H NMR (500 MHz, DMSO-d_6) d 2.58 (s, 3H, -$COCH_3$), 7.49 (dd, *J* = 8.1, 8.2 Hz, 1H, H-3), 7.86 (s, 1, H – 5), 7.97 (d, *J* = 9.0 Hz, 1H, H-7), 8.00 (d, *J* = 9.0 Hz, 1-H, H-8), 8.30 (d, *J* = 8.2 Hz, 1H, H-4), 8.76 (d, *J* = 8. ,1H, H-2), 10.98 (s, 1H, -NH), ^{13}C NMR (125 MHz, DMSO-d_6) d 25.9 (-$COCH_3$), 110.2 (C-5), 120.0 (C-7), 122.4 (C-3), 124.4 (C=N), 129.1 (C-4a), 130.7 (C-8), 135.7 (C-4), 141.0 (C-6), 145.1 (C-8a), 149.0 (C-2), 188.5 (-$COCH_3$), HRMS (ESI) calcd for $C_{12}H_{11}ClN_3O$ $[M+H]^+$ *m/z*: 248.05852, found 248.05789.

General procedure for the synthesis of Amidrazone (10a–l)

Compound **8** (0.65 g, 1.8 mmol) was suspended in ethanol (15 mL) at a temperature of 0 to -10 °C. A solution containing the appropriate secondary amine (2.2 mmol) and triethylamine (2 mL) in ethanol (5 mL) was added to the suspension with stirring. The stirring was continued at 0–5 °C for 2–4 h and then at room temperature overnight. The solvent was then removed under reduced pressure, and the resulting residue was treated with water (15 mL). The crude solid product was collected by suction filtration, washed with water, dried, and recrystallized using $CHCl_3$.

1-(Piperazin-1-yl)-1-(2-(quinolin-6-yl)hydrazineylidene)propan-2-one (10a)

Yield : 40.1%, brownish powder, mp 212 °C dec; R_f = 0.69 dichloromethane/methanol = 9.75:0.25 by volume). IR (KBr) n 1029, 1125, 1215, 1232, 1375, 1515, 1624, 1667, 2853 cm^{-1}; ^{1}H NMR (500 MHz, DMSO-d_6) d 2.41 (br.s, 1-H, H-4'), 2.46 (br.s, 3H, *Z/E*, -$COCH_3$), 2.98 (br.s, 4H, (H-3',H-5')), 3.21 (br.s, 4H, (H-2',H6')), 7.44 (br.s, 1H, H-3), 7.78 (s, 1H, H-5), 7.96 (br.s, 2H, (H-7, H-8)), 8.24 (br.s, 1H, H-4), 8.70 (br.s, 1H, H-2), 9.98, 10.07 (*Z/E*, 1H, -NH), ^{13}C NMR (125 MHz, DMSO-d_6) d 26.7 (-$COCH_3$), 47.7 (C-3',C-5'), 48.1 (C-2',C-6'), 109.0 (C-5), 120.3 (C-7), 122.3, 122.1 (*Z/E*, C-3), 129.4 (C-4a), 130.4, 130.5 (Z/E, C-8), 135.2 (C-4), 141.7, 141.9 (*Z/E*, C-6), 144.1 (C-8a), 144.7 (-C=N), 148.3 (C-2), 195.1, 195.3 (-$COCH_3$), HRMS (ESI) calcd for $C_{16}H_{19}N_5NaO$ $[M+Na]^+$ *m/z* : 320.14818, found 320.14509.

1-Morpholino-1-(2-(quinolin-6-yl)hydrazineylidene)propan-2-one (10b)

Yield: 91.3%, yellowish powder, mp 104 °C dec; R_f = 0.78 (dichloromethane/methanol = 9.75:0.25 by volume). IR (KBr) n 957, 974, 1033, 1066, 1111, 1206, 1234, 1279, 1334,1360, 1496, 1510, 1538, 1598, 1623, 1643, 2860, 3209, 3438 cm^{-1}; ^{1}H NMR (500 MHz, DMSO- d_6) d 2.40 (s, 3H, -$COCH_3$), 2.97 (br.s, 4H, (H-2', H-6')), 3.77 (br.s, 4H, (H-3', H-5')), 7.44 (dd, J = 8.3 , 8.3 Hz, 1H, H-3), 7.76 (s, 1H, H-5), 7.93 (d, *J* = 9.2 Hz, 1H, H-7), 7.95 (pst, 1H, H-8), 8.22 (d, *J* = 8.2 Hz, 1H, H-4), 8.69 (d, *J* = 4.00 Hz, 1H, H-2), 10.14 (s, 1H, -NH); ^{13}C NMR (125 MHz, DMSO-d_6) d 26.7 (-$COCH_3$), 47.7 (C-3',C-5'), 48.1 (C-2',C-6'), 109.0 (C-5), 120.3 (C-7), 122.3, 122.1 (*Z/E*, C-3), 129.4 (C-4a), 130.4, 130.5 (*Z/E*, C-8), 135.2 (C-4), 141.7, 141.9 (*Z/E*, C-6), 144.1 (C-8a), 144.7 (-C=N), 148.3 (C-2), 195.1, 195.3 (-$COCH_3$), HRMS (ESI) calcd for $C_{16}H_{19}N_4O_2$ $[M+H]^+$ *m/z* : 299.15025, found 299.14985.

1-(2-(Quinolin-6-yl)hydrazineylidene)-1-thiomorpholinopropan-2-one (10c)

Yield: 85.0%, Reddish powder, mp 160 – 162 °C; R_f = 0.78 (dichloromethane/methanol = 9.75:0.25 by volume). IR (KBr) n 947, 969, 1117, 1166, 1211, 1279, 1347, 1376, 1515, 1622, 1657, 2851, 2902, 3248 cm^{-1}; ^{1}H NMR (500 MHz, DMSO d_6) d 2.39 (s, 3H, -$COCH_3$), 2.81 (br.s, 4H, (H-3',H-5')), 3.16 (br.s, 4H, (H-2',H6')), 7.43 (dd, *J* = 8.3, 8.3 Hz, 1H, H-3), 7.76 (s, 1H, H-5), 7.94 (d, *J* = 1.8 Hz, 1H, H-7), 7.95 (d, *J* = 9.1 Hz, 1H, H-8), 8.20 (d, *J* = 8.2 Hz, 1H, H-4), 8.68 (d, *J* = 4.0 Hz, 1H, H-2), 10.06 (s, 1H, –NH); ^{13}C NMR (125 MHz, DMSO d_6) d 26.4 (-$COCH_3$),

27.5 (C-3',C-5'), 50.6 (C-2',C-6'), 109.2 (C-5), 120.5 (C-7), 122.5 (C-3), 129.3 (C-4a), 130.6 (C-8), 135.3 (C-4), 141.7 (C-6), 144.6 (C-8a), 144.7 (-C=N), 148.5 (C-2), 195.1 (-*C*OCH$_3$); HRMS (ESI) calcd for $C_{16}H_{19}N_4OS$ [M + H]$^+$ *m/z* : 315.12741, found: 315.12670.

Ethyl-4-(2-oxo-1-(2-(quinolin-6-yl)hydrazineylidene)propyl)piperazine-1- carboxylate (10d)

Yield: 85.7% , brownish powder, mp 125 °C dec; R_f = 0.88 (dichloromethane/methanol = 9.75:0.25 by volume). IR (KBr) n 967, 992, 1027, 1093, 1118, 1159, 1178, 1208, 1248, 1280, 1338, 1357, 1372, 1423, 1510, 1622, 1663, 1684 , 2854, 2923, 3247 cm^{-1}; ^{1}H NMR (500 MHz, DMSO d_6) d 1.19 (t, *J* = 7.1 Hz, 3H, -CH$_2$C*H*$_3$), 2.39 (s, 3H, -COCH$_3$), 2.92 (br.s, 2H , (H-2', H-6')), 3.56 (br.s , 2H, (H-3', H-5')), 4.07 (q, *J* = 7.1 Hz, 2H, -C*H*$_2$CH$_3$), 7.44 (dd, *J* = 8.3, 8.3 Hz, 1H, H-3), 7.75 (s, 1H, H-5), 7.92 (d, *J* = 9.2 Hz, 1H, H-7), 7.95 (d, *J* = 9.1 , 1H, H-8), 8.21 (d, *J* = 3 Hz, 1H, H-4), 8.69 (ps-t, 1H, H-2), 10.17 (s, 1H, -NH); ^{13}C NMR (125 MHz, DMSO d_6) d 15.0 (-CH$_2$*C*H$_3$), 26.3 (-CO*C*H$_3$), 44.0 (C-3', C-5'), 47.8 (C-2', C-6'), 61.3 (-*C*H$_2$CH$_3$), 109.1 (C-5), 120.3 (C-7), 122.4 (C-3), 129.3 (C-4a), 130.4 (C-8), 135.3 (C-4), 141.7 (C-6), 143.6 (-C=N), 144.7 (C-8a), 148.4 (C-2), 155.3 (-*C*O$_2$Et), 195.1 (-*C*OCH$_3$), HRMS (ESI) calcd for $C_{19}H_{24}N_5O_3$ [M + H]$^+$ *m/z* : 370.18737, found 370.18886.

1-(4′-(3″-Hydroxyphenyl)piperazin-1-yl)-1-(2-(quinolin-6- yl)hydrazineylidene) propan-2-one (10e)

Yield = 89.2%, Yellowish powder, mp 157–159 °C; R_f = 0.50 (dichloromethane/methanol = 9.75:0.25 by volume). IR (KBr) n 977, 996, 1034, 1188, 1231, 1264, 1332, 1372, 1452, 1509, 1545, 1579, 1625, 1670, 2856, 2936, 3271 cm^{-1}; ^{1}H NMR (500 MHz, DMSO-d_6) d 3.23 (s, 3H, -COCH$_3$), 3.85 (br.s, 4H, (H-2', H-6')), 4.03 (br.s , 4H, (H-3', H-5')), 6.96 (d , *J* = 7.9 Hz, 1H, H-6"), 7.10 (s, 1H, H-2"), 7.16 (d, *J* = 8.2 Hz, 1H, H-4"), 7.76 (ps-t, 1H, H-5"), 8.17 (dd, *J* = 8.3 , 8.3 Hz , 1H, H-3), 8.51 (s, 1H, H-5), 8.68 (br.s, 1H, H-7), 8.68 (br.s, 1H,H-8), 8.95 (d, *J* = 8.2 Hz, 1H, H-4), 9.43 (d, *J* = 2.75 Hz, 1H, H-2), 9.90 (br.s, 1H, OH), 10.84 (s , 1H, -NH), ^{13}C NMR (125 MHz, DMSO-d_6) d 26.4 (-CO*C*H$_3$), 47.8 (C-2',C-4'), 48.8 (C-3', C-5'), 103.1 (C-2"), 106.6 (C-6"), 107.2 (C-4"), 109.0 (C-5), 120.3 (C-7), 122.3 (C3), 129.4 (C-4a), 130.0 (C-5"), 130.4 (C-8), 135.2 (C-4), 141.8 (C-6), 143.9 (C-8a), 144.8 (-C=N), 148.3 (C-2), 153.1 (C-1"), 195.1 (-*C*OCH$_3$), HRMS (ESI) calcd for $C_{19}H_{24}N_5O_3$ [M + H]$^+$ *m/z*: 390.19245, found: 390.19316.

1-(4′-(4″-Nitrosophenyl)piperazin-1-yl)-1-(2-(quinolin-6- yl)hydrazineylidene) propan-2-one (10f)

Yield: 95.3%, yellowish powder, mp 177 °C dec; R_f = 0.88 (dichloromethane/methanol = 9.75:0.25 by volume). IR (KBr) n 965, 998, 1027, 1096, 1114, 1127, 1158, 1180, 1209, 1248, 1289, 1324, 1360, 1466, 1488, 1511, 1543, 1598, 1624, 1667, 2852, 3272 cm^{-1}; ^{1}H NMR (500 MHz, DMSO-d_6) d 2.40 (s, 3H, -COCH$_3$), 3.11 (br.s, 4H, (H-2', H-6'), 3.71 (br.s, 4H, (H-3', H-5')), 7.08 (d, *J* = 9.3 Hz, 2H, (H-2", H-6")), 7.45 (dd, *J* = 8.3, 8.3 Hz, 1H, H-3), 7.78 (s , 1H, H-5), 7.95 (d, *J* = 9.2 Hz, 1H, H-7), 7.99 (d, *J* = 9.1 Hz, 1H, H-8), 8.09 (d, *J* = 9.1, 2H, (H-3", H-5")), 8.23 (d, *J* = 8.3 Hz, 1H, H-4), 8.70 (d, *J* = 3.8 Hz, 1H, H-2), 10.23 (s, 1H, – NH), ^{13}C NMR (125 MHz, DMSO-d_6) d (ppm): 26.3 (-CO*C*H$_3$), 47.1 (C-2', C6'), 47.5 (C-3', C-5'), 109.1 (C-5), 113.1 (C-2", C-6"), 120.3 (C-7), 122.4 (C-3), 126.3 (C-3", C-5"), 129.3 (C-4a), 130.5 (C-8), 135.2 (C-4), 137.2 (C-4"), 141.8 (C-6), 143.4 (C=N), 144.8 (C-8a), 148.4 (C-2), 155.3 (C-1"), 195.1 (-*C*OCH$_3$), HRMS (ESI) calcd for $C_{19}H_{24}N_5O_3$ [M + H]$^+$ *m/z* : 419.18262 , found 419.18230.

1-(4′-(2″-Hydroxyphenyl)piperazin-1-yl)-1-(2-(quinolin-6-yl) hydrazineylidene) propan-2-one (10g)

Yield: 89.4%, Yellowish powder, mp 160 °C dec; R_f = 0.81 (dichloromethane/methanol = 9.75:0.25 by volume). IR (KBr). IR (KBr) n 1033, 1132, 1216, 1233, 1373, 1354, 1493, 1513, 1625, 1696, 2903, 2972, 3262 cm^{-1}; ^{1}H NMR (500 MHz, DMSO-d_6) d 2.43 (s, 3H, -COCH$_3$), 3.14 (br.s, 8H, (H-2', H-3', H-5', H6')), 6.81 (m, 2H, (H-4", H-5")), 6.82 (d, *J* = 7.2 Hz, 1H, H-6"), 6.94 (d, *J* = 7.2 Hz, 1H, H-3"), 7.44 (m, 1-H, H-3), 7.77 (s, 1H, H-5), 7.95 (br.s, 2H, (H-7, H-8)), 8.23 (d, *J* = 8.2 Hz, 1H, H-4), 8.70 (br.s, 1H, H-2), 9.02 (s, 1H, -OH), 10.10 (s, 1H, -NH), ^{13}C NMR (125 MHz, DMSO-d_6) d 26.4 (-CO*C*H$_3$), 48.1 (C-2', C-6'), 50.6 (C-3', C-5'), 109.0 (C-5), 116.1 , 119.1 (C-5", C-6"), 119.8 (C-3"), 120.3 (C-7), 122.4 (C-3), 123.4 (C-4"), 129.3 (C-4a), 130.4 (C-8), 135.2 (C-4), 140.7 (C-2"), 141.8 (C-6), 144.2 (C-8a), 144.5 (-C=N), 148.3 (C-2), 150.6 (C-1"), 195.2 (-*C*OCH$_3$), HRMS (ESI) calcd for $C_{22}H_{24}N_5O_2$ [M + H]$^+$ *m/z* : 390.19245, found 390.19326.

1-(4′-(4″-Chlorophenyl)piperazin-1-yl)-1-(2-(quinolin-6- yl)hydrazineylidene) propan-2-one (10h)

Yield: 91.1%, Brownish powder, mp 151–153 °C; R_f = 0.88 (dichloromethane/methanol = 9.75:0.25 by volume). IR (KBr) n 964, 1005, 1228, 1117, 1156, 1215, 1234, 1317, 1358, 1457, 1496, 1510, 1669, 2850, 2922, 3271 cm^{-1}; ^{1}H NMR (500 MHz, DMSO-d_6) d 2.42 (s, 3H, -COCH$_3$) , 3.11 (br.s, 4H, (H-2' , H-6')), 3.33 (br.s , 4H , (H-3' , H-5')), 7.00 (d, *J* = 8.4 Hz, 2H, (H-2", H-6")), 7.26 (d, *J* = 8.6 Hz, 2H, (H-3", H-5")), 7.45 (dd, *J* = 8.2, 8.3 Hz, 1H, H-3), 7.77 (s, 1H, H-3), 7.94 (d, *J* = 9.3 Hz, 1H, H-7), 7.95 (d, *J* = 9.0 Hz, 1H, H-8), 8.21 (d, *J* = 8.1, 1H, H-4), 8.70 (br.s, 1H, H-2), 10.12 (s, 1H, -NH), ^{13}C-NMR (125 MHz, DMSO-d_6) d (ppm): 26.4 (-CO*C*H$_3$), 47.7 (C-2', C-6'), 48.6 (C-3', C-5'), 109.0 (C-5), 117.4 (C-2",C-6"), 120.3 (C-7), 122.3 (C-4"), 122.7 (C-3), 129.1 (C-3", C-5", C4a), 130.4 (C-8), 135.2 (C-4), 141.8 (C-6), 143.8 (C-8a), 144.8 (-C=N), 148.4 (C-2), 150.5 (C-1"), 195.2 (-*C*OCH$_3$), HRMS (ESI) calcd for $C_{22}H_{23}{}^{35}ClN_5O$ [M+H]$^+$ *m/z* : 408.15856, found 408.15764.

1-(4′-Phenylpiperazin-1-yl)-1-(2-(quinolin-6-yl)hydrazineylidene)propan-2-one (10i)

Yield = 88.0%, Brownish powder, m.p. 135–137 °C; R_f = 0.88 (dichloromethane/methanol = 9.75:0.25 by volume). IR (KBr) n 991, 1027, 1131, 1159, 1231, 1259, 1328, 1378, 1449, 1491, 1504, 1534, 1596, 1624, 1666, 2826,

2921, 3268 cm^{-1}; ^1H NMR (500 MHz, DMSO d_6) d 2.49 (s, 3H, -$COCH_3$), 3.13 (br.s, 4H, (H-2', H-6')), 3.35 (br.s, 4H, (H-3', H-5')), 6.79 (br.s, 1H, H-4"), 6.96 (d, *J* = 6.8 Hz, 2H, (H-2", H-6")), 7.23 (br.s, 2H, (H-3", H-5"), 7.44 (br.s, 1H, H-3), 7.79 (s, 1H, H-5), 7.96 (s, 1H, H-7), 7.97 (s, 1H, H-8), 8.22 (d, *J* = 7.35 Hz, 1H, H-4), 8.70 (br.s, 1H, H-2), 10.12 (s, 1H, -NH), ^{13}C NMR (125 MHz, DMSO d_6) d 26.4 (-$COCH_3$), 47.8 (C-2', C-6'), 48.8 (C-3', C-5'), 109.0 (C-5), 116.0 (C-2", C-6"), 119.2 (C-4"), 120.3 (C-7), 122.3 (C-3), 129.4 (C-4a, C-3", C-5"), 130.5 (C-8), 135.2 (C-4), 141.8 (C-6), 143.9 (C-8a), 144.8 (-C=N), 148.3 (C-2), 151.8 (C-1"), 195.1 (-*C*OCH_3), HRMS (ESI) calcd for $C_{22}H_{24}N_5O$ $[M + H]^+$ *m/z* : 374.19754, found 374.19660.

1-(4'-(4''-Hydroxyphenyl) piperazin-1-yl)-1-(2-(quinolin-6- yl) hydrazono)propan-2-one (10j)

Yield: 92.6%, brownish powder, mp 161–163 °C; R_f = 0.46 (dichloromethane/methanol = 9.75:0.25 by volume). IR (KBr) n (cm^{-1}): 955, 1034, 1134, 1230, 1375, 1451, 1512, 1620, 1675, 2947, 3257 cm^{-1}; ^1H NMR (500 MHz, DMSO d_6) d 2.49 (s, 3H, -$COCH_3$), 3.07 (br.s, 4H, (H-3', H-5')), 3.12 (br.s, 4H, (H-2', H-6')), 6.67 (d, *J* = 8.7 Hz, 2H, (H-2", H-6")), 6.82 (d, *J* = 8.2 Hz, 1H, (H-3", H-5")), 7.44 (dd, *J* = 8.3, 8.2 Hz , 1H, H-3), 7.77 (s, 1H, H-5), 7.95 (ps.t, 2H, (H-7, H-8)), 8.21 (d, *J* = 8.2 Hz, 1H, H-4), 8.69 (d, *J* = 2.75 Hz, 1H, H-2), 8.82 (s,1H,OH), 10.05 (s, 1H, NH): ^{13}C NMR (125 MHz, DMSO d_6) d 26.5 (-$COCH_3$), 48.0 (C-2'), 50,6 (C-3'), 109.0 (C-5), 115.9 (C-2", C-6"), 118.5 (C-3", C-5"), 120.3 (C-7), 122.3 (C-3), 129.4 (C-4a), 130.4 (C-8), 135.2 (C-4), 141.8 (-C=N), 144.0 (C-8a), 144.7 (C-4"), 145.0 (C-6), 148.3 (C-2), 151.4 (C-1"), 195.1 (-*C*OCH_3); HRMS (ESI) calcd for $C_{22}H_{24}N_5O_2$ $[M + H]^+$ *m/z* : 390.19245, found 390.19429.

1-(4'-Phenylpiperazin-1-yl)-1-(2-(quinolin-6-yl)hydrazineylidene)propan-2-one (10k)

Yield: 89.1%, yellowish powder, mp 135–137 °C; R_f = 0.73 (dichloromethane/methanol = 9.75:0.25 by volume). IR (KBr) n 935, 1027, 1130, 1206, 1232, 1259, 1314, 1326, 1355, 1389, 1454, 1512, 1554, 1591, 1645, 1627, 2865, 3211, 3408 cm^{-1}; ^1H NMR (500 MHz, DMSO-d_6) d 2.41 (s, 3H, -$COCH_3$), 3.02 (br.s, 4H, (H-3',H-5')), 3.96 (br.s, 4H, (H-2',H6')), 6.63 (br.s, 1H, H-5"), 7.44 (d, *J* = 3.9 Hz , 1H, H-3), 7.78 (s, 1H, H-5), 7.95 (br.s, 1H, H-7), 7.97 (br.s, 1H, H-8), 8.22 (d, *J* = 7.9 Hz, 1H, H-4),8.37 (d, *J* = 7.9 Hz, 2H, (H-4", H-6")), 8.70 (br.s, 1H, H-2), 10.22 (s, 1H, -NH), ^{13}C NMR (125 MHz, DMSO-d_6) d (ppm): 26.7 (-$COCH_3$), 44.0 (C-2',C-6'), 47.7 (C-3',C-5'), 109.1 (C-5), 110.5 (C-5"), 120.3 (C-7), 122.3 (C-3), 129.4 (C-4a), 130.4 (C-8), 135.2 (C-4), 141.8 (C-6), 143.8 (C-8a), 144.8 (-C=N), 148.4 (C-2),158.4 (C4", C-6"), 161.8 (C-2"), 195.1 (-*C*OCH_3), HRMS (ESI) calcd for $C_{20}H_{22}N_7O$ $[M + H]^+$ *m/z* : 376.18803, found 376.18988.

1-(4'-(pyridin-2-yl)piperazin-1-yl)-1-(2-(quinolin-6-yl)hydrazineylidene)propan-2-one (10l)

Yield: 92.0%, yellowish powder, mp 125–127 °C; R_f = 0.79 (dichloromethane/methanol = 9.75:0.25 by volume). IR (KBr) n 957, 977, 1026, 1124, 1179, 1227, 1255, 1329, 1489, 1528, 1602, 1656, 2855, 3266 cm^{-1}; ^1H NMR (500 MHz, DMSO- d_6) d 2.42 (s, 3H, -$COCH_3$), 3.06 (s, 2H, (H-2', H-6')), 3.71 (s, 2H, (H-3', H-5')), 6.64 (br.s, 1H, H-5"), 6.85 (d, *J* = 8.4 Hz, 1H, H-3"), 7.43 (br.s, 1H, H-3), 7.53 (t, *J* = 8.2 Hz, 1H, H-4"), 7.78 (s, 1H, H-5), 7.95 (d, *J* = 9.1 Hz, 1H, H-7), 7.97 (d, *J* = 9.0 Hz, 1H, H-8), 8.13 (br.s, 1H, H-6"), 8.22 (d, *J* = 8 Hz, 1H, H-4), 8.70 (br.s, 1H, H-2), 10.17 (s, 1H, – NH), ^{13}C NMR (125 MHz, DMSO-d_6) d 26.4 (-$COCH_3$), 45.3 (C-2', C6'), 47.6 (C-3', C-5'), 107.6 (C-3"), 109.0 (C-5), 113.3 (C-5"), 120.3 (C-7), 122.3 (C-3), 129.4 (C-4a), 130.5 (C-8), 135.2 (C-4), 138.0 (C-4"), 141.8 (C-6), 143.9 (C=N), 144.8 (C-8a), 148.1 (C-6"), 148.3 (C-2), 159.6 (C-2"), 195.1 (-$COCH_3$), HRMS (ESI) calcd for $C_{21}H_{23}N_6O$ $[M + H]^+$ *m/z* :375.19279, found 375.19116.

Molecular modeling

Computational docking

The synthesized compounds **(10a–l)** were docked into the active site of c-Abl kinase. The 3D coordinates of the c-Abl kinase with known co-crystallized pyrimidine inhibitor (STI-571), were retrieved from Protein Data Bank (c-Abl, PDB code: 1IEP, resolution: 2.10 Å). First, the protein was prepared by adding hydrogen atoms using Biovia Discovery Studio software 4.5. The protein was cleaned, prepared, and repaired by adding missing atoms, correcting connectivity and names, and inserting missing loops. Secondly, the active site was defined around the co-crystallized ligand (STI-571) using the (From Current Selection) option of the (Define and Edit Binding Site) tool in Biovia Discovery Studio 4.5, shown in (Fig. 4). The co-crystallized ligand (STI-571) was removed from the binding site for docking validation. The ligand was redocked using the LibDock algorithm and the Root Mean Square Deviation (RMSD) was calculated to validate and assess pose similarity between the ligand poses concerning the original pose of the ligand. The RMSD value for the pose with the highest LibDock scores in comparison to the co-crystallized pose was 2.1Å (around 2Å) which is acceptable. The final amidrazone-quinoline compounds bearing 6-aminoquinoline moiety in their structures were docked into the binding site of the selected c-Abl kinase using the default LibDock algorithm.

Ligand preparation for LibDock

The site-feature docking algorithm (LibDock) docks ligands, after removing their hydrogen atoms, into an existing active site as guided by binding hotspots. The ligands' conformations are aligned to polar and apolar receptor interaction sites (i.e., hotspots). Conformations can be either pre-calculated or generated on the fly. Optionally, a CHARMm minimization step can be enabled to further optimize docked poses. Docking with LibDock has several steps which can be summarized in: (i) removal of hydrogen atoms. (ii) Ranking ligand conformations and prun-

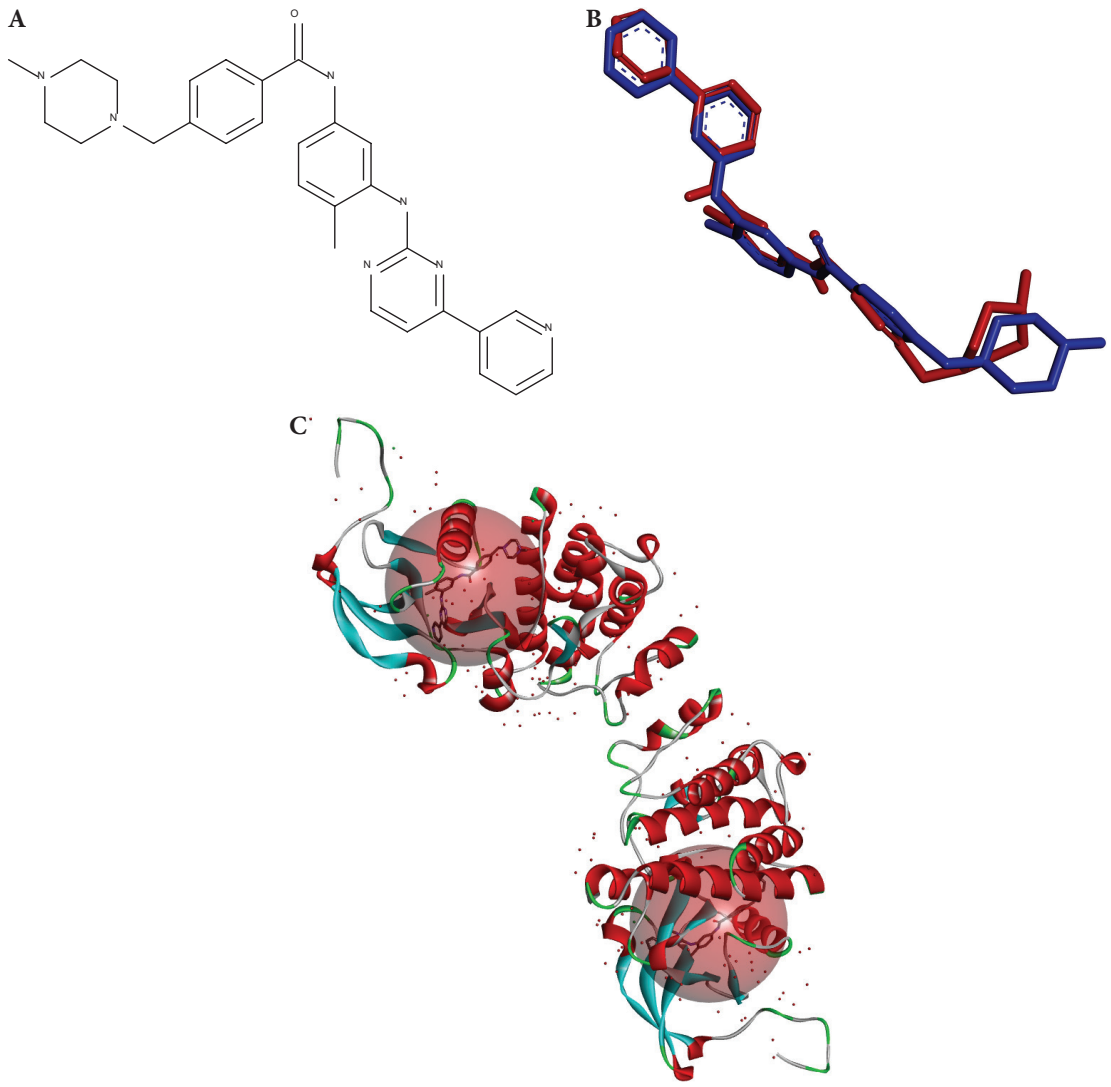

Figure 4. A. The co-crystallized pyrimidine ligand (1IEP); **B.** The co-crystallized pose and the docked pose of the co-crystallized ligand with RMSD = 2.10 Å; **C.** The binding site of the c-Abl-kinase protein (PDB code: 1IEP, resolution: 2.10 Å). Blue is for the co-crystal compounds, and red is for the highest Libdock score compound (Libdock score = 169.76).

ing by solvent-accessible surface area (SASA). (iii) Finding hotspots using a grid that is placed into the binding site and using polar and apolar probes. (iv) The number of hotspots is trimmed by clustering to a user-defined value. (v) Docking of ligand poses by aligning the binding site hotspots, performed by using triplets (three ligand atoms are aligned to three receptor hotspots). (vi) a final BFGS pose optimization stage is performed using a simple pairwise score (similar to Piecewise Linear Potential). (vii) The top-scoring ligand poses are retained. (viii) Hydrogen atoms are added back to the docked ligands. (ix) Optionally CHARMm minimization can be carried out to reduce steric clashes caused by added hydrogen atoms. The following LibDock parameters were applied in the current study: Before docking, the Biovia 4.5 module CAT-CONFIRM was used to generate a maximum of 250 conformers (not exceeding an energy threshold of 20 kcal/mol from the most stable conformer) for each ligand employing "Fast" conformation generation option. A binding site sphere of 12.77 Å radius surrounding the center of the co-crystallized ligand (STI-571) was retrieved from Protein Data Bank (c-Abl, PDB code: 1IEP, resolution: 2.10 Å) and was used to define the binding site. The number of binding site hotspots (polar and apolar) was set to 100. The ligand-to-hotspots matching RMSD tolerance value was set to 0.25 Å. The maximum number of poses saved for each ligand during hotspots matching before final pose minimization = 100. Maximum number of poses to be saved for each ligand in the binding pocket = 100. Minimum LibDock score (poses below this score are not reported) = 100. Maximum number of rigid body minimization steps during the final pose optimization (using BFGS method) = 50. The maximum number of steric clashes allowed before the pose-hotspot alignment is terminated (specified as a fraction of the heavy atom count) = 0.1. Maximum value for nonpolar solvent accessible surface area for a particular pose to be reported as successful = 15.0 Å2. Maximum value for polar solvent accessible solvent area for a particular pose to be reported as successful = 5.0 Å2. No final ligand minimization was implemented (i.e., in the binding pocket).

Toxicity prediction using EC_{50} Daphnia calculations

Toxicity prediction studies were performed using software suites implemented in Discovery Studio 4.5 from Biovia Inc. (San Diego, California, Structures were drawn by ChemDraw Ultra 7.0 (Cambridge Soft Corp. (http://www.cambridgesoft.com), USA).

Data set

The synthesized compounds **10a–l** were analyzed using the default parameters in Biovia 4.5 using the TOPKAT toxicity function after the addition of all parameters.

In vitro anticancer screening

Cells were seeded in 96-well plates at a density of 8×10^3 and 5×10^3, cells per well in the appropriate medium for A549 and MCF-7 cell lines, respectively. For screening anti-MCF7 anti-A549, the desired concentrations of the tested compounds were applied to the cells. For IC_{50} determination, the cells were treated with increasing concentrations of the tested compound, ranging from 1.00 to 1000 µM. The drugs were dissolved in DMSO before being added to cell cultures, and equal amounts of the solvent were added to control wells. After 48 h of treatment, 10 µL of MTT dye (working concentration of 5 mg/mL) was added to each well, and the plates were further incubated for 4 hours. Afterward, the media was discarded and 100 µL of DMSO was added to the wells. Optical density was measured at 570 nm and 630 nm with a microplate reader (µ Quant Plate Reader, Biotek, USA). All experiments were repeated in triplicate wells and on at least their independent occasions. Dose-response curves were used to obtain IC_{50} concentrations based on the following Equation:

Equation 1. Cell viability calculation.

$$\text{Cell viability}\ (\%) = \frac{\text{Optical density of treated cells}}{\text{optical density of untreated cells}} \times 100$$

Data were analyzed using Graph Pad Prism Software 9 from San Diego, California, USA (www.graphpad.com).

Collection of X-ray diffraction data and structure analysis of compound (10b)

The slow growth of orange block crystals from a dilute **10b** Methanol solution took place over one week. Using epoxy glue, a suitable crystal with approximate dimensions of $0.3 \times 0.1 \times 0.1$ mm^3 was mounted onto a glass fiber and then data were collected at room temperature (293 K) *via* the Oxford Xcalibur diffractometer. The CrysAlis Pro software (CrysAlisPro, Oxford Diffraction Ltd., Version 1.171.35.19 (release 27-10-2011 CrysAlis171.NET) was employed to acquire and process the data. The crystal was kept at 293(2) K during data collection. Using Olex2, the structure was solved with the SHELXT structure solution program using Intrinsic Phasing and refined with the SHELXL (Sheldrick 1996; Sheldrick 2015a, 2015b) refinement package using Least Squares minimization. No hydrogen atoms were refined anisotropically with hydrogen atoms positioned using a riding model. A summary of the crystallographic data can be found in (Table 1). The supplementary crystallographic data for this paper can be obtained free of charge from The Cambridge Crystallographic Data Centre via www.ccdc.cam.ac.uk/data_request/cif, with the CCDC 2257301 code.

Table 1. Crystal data and structure refinements for compound **10b**.

Empirical formula	$C_{16}H_{22}N_4O_4$
Formula weight, g mol^{-1}	334.37
Temperature, K	293(2)
Wavelengthλ, Å	0.71073
Crystal system	Triclinic
Space group	P1
a, Å	5.2960(3)
b, Å	9.3134(6)
c, Å	9.4794(7)
α/°	106.359(6)
β/°	102.219(5)
γ/°	94.535(5)
Volume, Å^3	433.65(5)
Z	1
Density (calcd.), g cm^{-3}	1.28
Absorption coefficient μ, mm^{-1}	0.094
F(000), *e*	178
2θrange for data collection, deg	7.46–58.564
Index ranges*hkl*	$-6 \le h \le 7$, $-11 \le k \le 12$, $-12 \le l \le 11$
Reflections collected	6705
Independent reflections	3912
R(*int*)	0.0231
Absorption correction	Semi-empirical from equivalents
Refinement method	Full-matrix least-squares on F^2
Data / restraints / parameters	3912 / 3 / 232
$R1^a$ / $wR2^b$ [$I > 2$ sigma > (I)]	0.0499 / 0.1005
$R1^a$ / $wR2^b$(all data)	0.0892 /0.1224
Goodness-of-fit on F^2	1.026
Largest diff. peak/hole, eÅ^{-3}	0.12 / -0.17

$^aR1 = \Sigma||Fo| - |Fc||/\Sigma|Fo|$; $^bwR2 = [\Sigma w(F_o^2 - F_c^2)^2/\Sigma w(F_o^2)^2]^{1/2}$.

Results and discussion

Chemistry

In this study, the hydrazonoyl chloride **8** was synthesized by directly coupling the respective quinoline-6-diazonium chloride with 3-chloroethane-2,4-dione in an aqueous alcoholic sodium acetate solution using the Japp-Klingemann reaction (Scheme 1) as per previously documented methods (Yao et al. 1962). To prepare the quinoline-6-diazonium chloride, freshly diazotized the respective 6-aminoquinoline **6** (suspended in 6 N aq. HCl). The resulting hydrazonoyl chloride precursor **8** was expected to undergo nucleophilic addition reactions with piperazines and the related sec-cyclic amine congeners **9a–l**, acting as nitrogen nucleophiles, resulting

in the formation of the respective amidrazone adducts **10a–l** (Scheme 2). This reaction mechanism has been extensively documented (Ulrich 1968; Butler et al. 1970; Benincori and Sannicoló 1988; Habashneh et al. 2014; Abdullah et al. 2016). The newly synthesized compounds were identified and characterized using MS and NMR spectral data, as detailed in the experimental section. The data revealed consistent results supporting the proposed structures. Specifically, the mass spectra displayed the correct molecular ion peaks, and the high-resolution mass spectral data agreed well with calculated values. DEPT and 2D (COSY, HMQC, and HMBC) experiments also helped with signal assignments for the different carbons and their attached and neighboring hydrogens. We confirmed the structures by single crystal X-ray structure determination for **10b** (Fig. 4), representing the series.

X-ray structure determination of (10b)

X-ray crystal structure determination was performed to confirm the structure of **10b** (Scheme 2) as a representative example of the new synthetic *N*-(quinolin-6-yl) amidrazones **10a–l**. A summary of data collection and refinement parameters is given in Table 1. The molecular structure of **10b** in the crystal is shown in (Fig. 5). **10b** crystallizes as dihydrate. The mean plane of the quinoline is nearly perpendicular to the plane of the rest of the molecule. Water molecules are linked via O-H···O hydrogen bonding interactions to form a chain structure that runs parallel to the crystallographic *a*-axis (Fig. 6-top). Subsequently, these layers are linked via C-H···O hydrogen bonding interactions to form tunneled framework structures; these tunnels are filled with water molecules (Fig. 6-bottom).

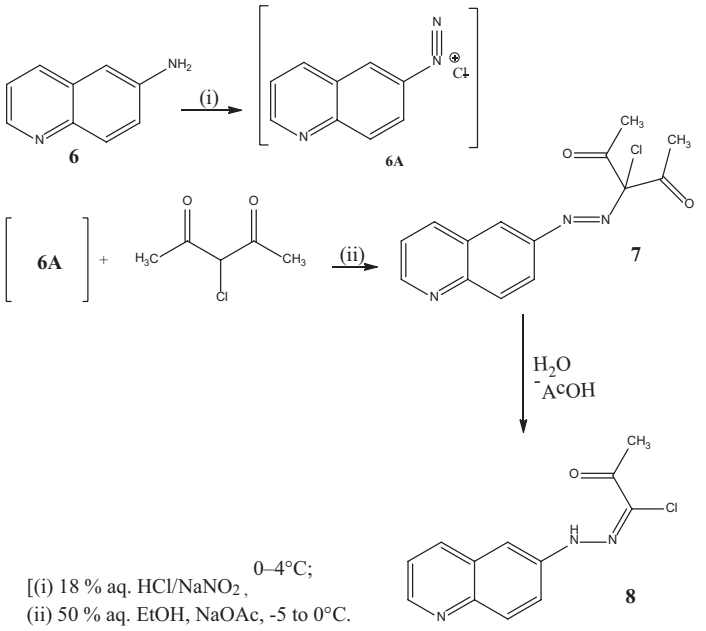

Scheme 1. Synthetic route to compound **8**.

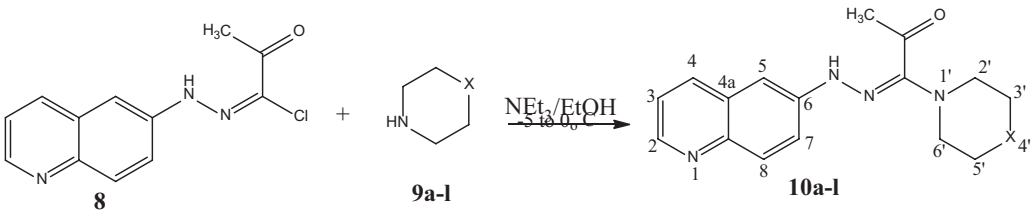

Compound	**10a**	**10b**	**10c**	**10d**	**10e**	**10f**
X	NH	O	S		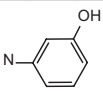	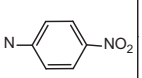
Compound	**10g**	**10h**	**10i**	**10j**	**10k**	**10l**
X	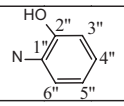	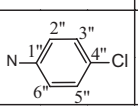	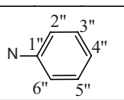	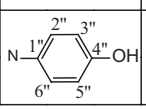	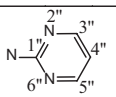	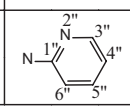

Scheme 2. Synthetic route for compounds **10a–l**.

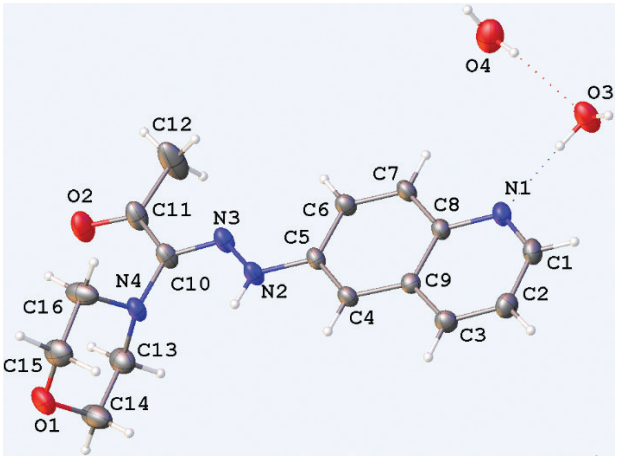

Figure 5. X-ray structure of **10b**.

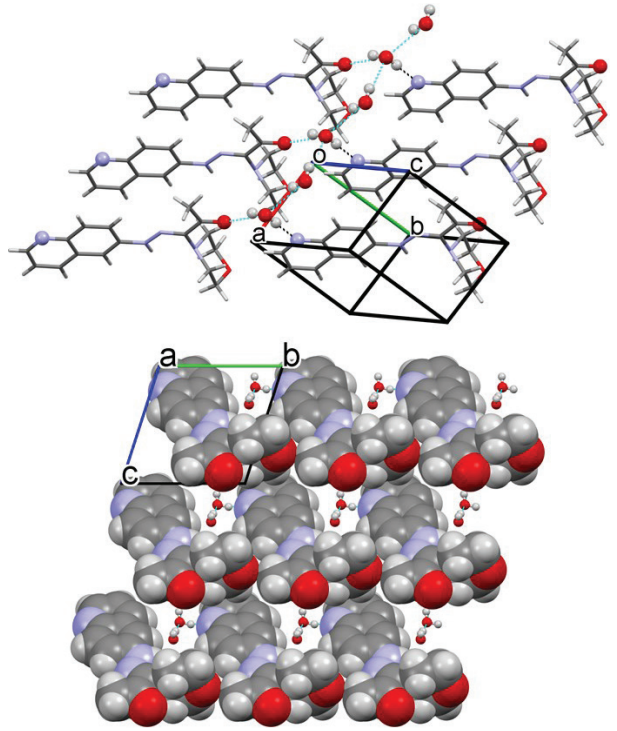

Figure 6. Layer structure of **10b** (top) and the three-dimensional structure of **10b** (bottom).

Computational docking

According to computational docking, a small chemical attaching to a larger receptor should form a stable complex (Khamis et al. 2015). Molecular docking is one of the best in silico methods for predicting chemical-biological target interactions (Kitchen et al. 2004). Diller and Merz's LibDock algorithm directs docking using protein binding sites (Diller et al. 2001). The LibDock technique involves constructing the ligand's conformations, finding polar and apolar hot spots, matching the binding site picture with the ligand, and optimizing and scoring (Rao et al. 2007). Docking's ability to identify active molecules from decoys depends on the protein and the co-crystallized ligand's similarity to the screened ligands (Al-Sha'er et al. 2015; Al-Sha'er et al. 2016; Al-Sha'er et al. 2019; Al-Sha'er et al. 2022). We selected the protein data bank file (1IEP, resolution: 2.10 Å) based on the provided information. Pyrimidine ligand and c-Abl kinase co-crystallized (STI-571) are included. By calculating the RMSD, the difference between the best-docked posture and the initial co-crystallized pose, the LibDock score (169.76) was used to choose the best stance conformation to confirm docking. An RMSD of 2.10Å was observed. As shown in (Fig. 6), the co-crystallized ligand (STI-571) forms four hydrogen bonds with the c-Abl kinase enzyme's binding site amino acids: Met318 with the heteroatom N in the pyridinyl group, Thr315 with the NH_2, Asp381 with the carbonyl (C=O) of the amide bond, and Met290 with the NH-. All resulting synthetic compounds have acceptable LibDock scores compared to the co-crystallized ligand, which had 1–5 hydrogen bonds. The two-dimensional study (Fig. 4) shows that the selected chemicals may bind to the c-Abl enzyme via hydrogen bonding, dipole-dipole interactions, charge transfer, and Van der Waal interactions with hydrophobic amino acids.

(Fig. 7) shows the predicted interaction of the most active substance (**10d**; libDock score: 123.46) with the c-Abl kinase binding site via three hydrogen bonds: Glu316 with phenolic OH, Met318 with phenolic OH group, Glu286 with NH-amidrazone, and ASP381 with quinoline ring via π-π aromatic stacking. The suggested work will be screening synthetic compounds (**10d** and **10g**) for anti-c-Abl kinase activity at 100 μM using Invitrogen Thermo Fisher Scientific Enzyme assay service (Kashem et al. 2007). Most compounds had lower LibDock scores than the co-crystallized ligand (STI-571). The site feature technique (LibDock) has numerous shortcomings because it is mostly used to rapidly dock combinatorial libraries of compounds to prioritize library selection above compound rank sorting. The lack of concordance between docking data and in vitro enzymatic activity is one. Another issue in computational chemistry is protein-ligand affinity prediction accuracy (Meng et al. 2011). However, protein systems score differently, and projections often don't match experimental evidence (Warren et al. 2006; Rao et al. 2007; Verdonk et al. 2008; Cheng et al. 2009). The targeted chemicals **10a–l** may fight cancer without inhibiting c-Abl kinase. After numerous research studies introduced amidrazone compounds as anti-cancer agents, further chemical modification to improve activity and safety and exploration of various suggested mechanisms of anticancer activity are essential. Additionally, the toxicity profile suggests that amidrazone-quinoline derivatives may be toxic to Daphnia with low EC50 values, emphasizing the need for in vivo evaluation.

ADMET and Daphnia magna EC_{50}

The chemicals were assessed using Biovia 4.5's default parameters for absorption, distribution, metabolism, and excretion, then the TOPKAT toxicity function after adding all parameters. As shown in (Fig. 8), all synthetic amidrazone derivatives have acceptable pharmacokinetic characteristics.

AQUIRE provided this TOPKAT model's data citations. After reading each source, Daphnia magna EC50 values were determined. Models were created from 48-

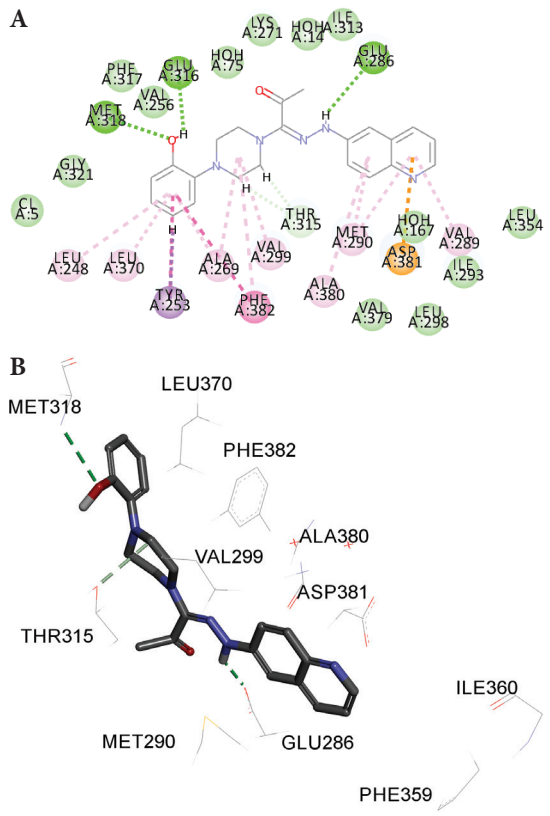

Figure 7. A. Diagram of receptor-ligand interaction between compound (**10d**) and c-Abl kinase (PDB code: 1IEP); **B.** 3D diagram of receptor-ligand interaction between compound (**10d**) c-Abl kinase enzyme (PDB code: 1IEP).

hour tests. Open-beaker volatile chemical tests were not used. For substances with multiple assay values, the median was used. The acute aquatic toxicity model calculates the EC50 of a drug that harms 50% of the Daphnia magna test population within a given time (Persoone et al. 2009; Biovia 2016).

(Table 3) shows that compound **10d**, the most potent MTT molecule, is non-carcinogenic with EC50 = 0.11 mg/L (Table 2), but high Daphnia toxicity suggests that synthetic amidrazone derivatives should be tested in vivo.

TOPKAT uses a Quantitative Structure-Toxicity Relationship (QSTR) equation to estimate toxicity for a chemical structure. Structure descriptors show a linear equation. Coefficients are optimized during equation formulation. Structure descriptors contribute to likely toxicity by multiplying their value by their coefficient. Positive product contributions raise the probability of the desired property, whereas negative contributions decrease it. Summing up individual contributions yields toxicity values. This total is converted to mg/kg or mg/l for toxicity values like LD_{50} or LC_{50}.

Two-group linear discriminant analysis is used in all QSTR models with two-group classifications, such as carcinogens/non-carcinogens. Discriminant function employs a linear combination of descriptor variables to identify circumstances as carcinogenic or not. The compound function determines the discriminant score. As positive discriminants increase, toxicity probabilities approach 1. The more negative the discriminant, the closer toxicity is to 0. Total descriptor contributions equals discriminant scores. Enter smiles, choose a model, and check the "descriptor contribution" window for each descriptor's report window contributions in stand-alone TOPKAT. The compound descriptor times model coefficient is shown in the descriptor contribution window. Coefficients are unavailable. If a discriminant score is positive, it indicates a toxic compound (carcinogen, mutagen, etc.), while if it is negative, it indicates a non-toxic compound. Instead of the discriminant score, utilize the Computed Probability to determine toxicity. Between 0 and 0.29, the molecule is non-toxic, between 0.3 and 0.69, it is uncertain, and between 0.7 and 1, it is poisonous (Drews 2000; Alelaimat et al. 2023).

Antiproliferative activity

Cell viability assays using tetrazolium dye 3-(4,5-dimethylthiazol-2-yl)-2,5-diphenyltetrazolium bromide (MTT) were performed to characterize the antitumor activity of the newly synthesized amidrazones (**10a–l**/Scheme 2). The breast cancer cell line MCF-7 and the lung cancer cell line A549 were treated with varying concentrations, and the resulting IC_{50} values are provided in (Table 3).

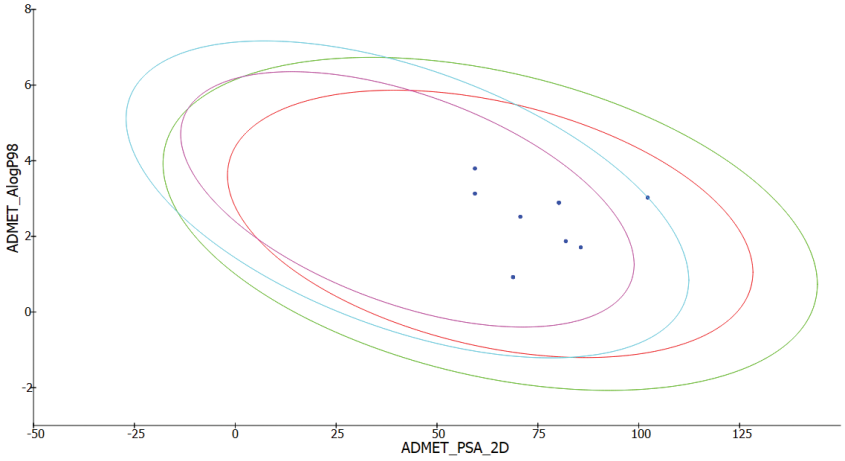

Figure 8. ADME analysis of synthetic amidrazone structures (blue dot).

Table 2. Toxicity and Carcinogenic predicted properties of amidrazone derivatives.

Compound No.	Daphnia EC50mg/L*	Carcinogenicity#
10a.mol	0.54	Carcinogen
10b.mol	0.1	Non-Carcinogen
10c.mol	0.03	Non-Carcinogen
10d.mol	0.11	Non-Carcinogen
10e.mol	0.02	Non-Carcinogen
10f.mol	0.04	Non-Carcinogen
10g.mol	0.12	Non-Carcinogen
10h.mol	0.04	Non-Carcinogen
10i.mol	0.12	Non-Carcinogen
10j.mol	0.11	Non-Carcinogen
10k.mol	0.07	Carcinogen
10l.mol	0.42	Carcinogen

* EC50; effective concentration that kills 50% of daphnia;
#TOPKAT_Rat_Male_FDA_None_vs_Carcinogen_Prediction.

Table 3. MTT assay for the synthetic compounds **10 a–l**.

Compound	IC_{50} μM(A549)#	IC_{50} μM(MCF-7)#
10a	482.6	317
10b	320.2	539
10c	96	95.2
10d	43.1	59.1
10e	150.3	191.7
10f	862.9	1127
10g	59.23	63.5
10h	370.6	350
10i	127	140.9
10j	499.1	496.2
10k	280.5	254
10l	529.3	697
Cisplatin*	22	-
Doxorubicin**	-	5

#IC_{50} values expressed as uM; SD never exceeded 5% (n=9). Treatment for 48 h; *positive control for lung cancer A549; **Positive control for breast cancer MCF7.

Conclusions

The study reports synthesizing and testing a new series of compounds derived from 6-aminoquinoline and piperazine for their potential antitumor activity against breast and lung cancer cell lines (MCF-7 and A549). The compounds were synthesized by reacting the hydrazonoyl chloride derived from 6-aminoquinoline with the appropriate piperazine. The results of the in vitro tests showed that all of the compounds had weak antitumor activity against the tested cell lines, with compounds **10d** and **10g** exhibiting the most promising activity with IC_{50} values of 43.1 μM and 59.1 μM against A549 and MCF-7 cell lines, respectively.

Docking on the binding site of the c-Abl kinase enzyme suggests that the mechanism of antitumor effect may be due to the enzyme inhibition, further, ADMET *in silico* studies showed acceptable pharmacokinetic properties while the most active hits as possibly highly toxic with Daphnia EC_{50} 0.11 and 0.12 mg/L so further in vivo evaluation of the safety profile is necessary for the development of the new safe, non-carcinogenic lead compounds.

Acknowledgments

The authors would like to express their gratitude to the Deanship of Scientific Research at Zarqa University and the University of Jordan for their generous funding.

Zarqa University's Scientific Research Department provided funding for Ahmad K. Alarareh's master's project under fund code 5-2(3/2021).

References

Abdullah AH, Zahra JA, El-Abadelah MM, Sabri SS, Khanfar MA, Matar SA, Voelter W (2016) Synthesis and antibacterial activity of *N*1-(carbazol-3-yl)amidrazones incorporating piperazines and related congeners. Zeitschrift für Naturforschung B 71: 857–867. https://doi.org/10.1515/znb-2016-0043

Alelaimat MA, Al-Sha'er MA, Basheer HA (2023) Novel sulfonamide–triazine hybrid derivatives: Docking, synthesis, and biological evaluation as anticancer agents. ACS Omega 8: 14247–14263. https://doi.org/10.1021/acsomega.3c01273

Al-Sha'er MA, Al-Aqtash RA, Taha MO (2019) Discovery of new phosphoinositide 3-kinase delta (PI3Kδ) inhibitors via virtual screening using crystallography-derived pharmacophore modelling and QSAR analysis. Journal of Medicinal Chemistry 15: 588–601. https://doi.org/10.2174/1573406415666190222125333

Al-Sha'er MA, Basheer HA, Taha MO (2022) Discovery of new PKN2 inhibitory chemotypes via QSAR-guided selection of docking-based pharmacophores. Molecular Diversity 27: 443–462. https://doi.org/10.1007/s11030-022-10434-4

Al-Sha'er MA, Mansi I, Almazari I, Hakooz N (2015) Evaluation of novel Akt1 inhibitors as anticancer agents using virtual co-crystallized pharmacophore generation. Journal of Molecular Graphics and Modelling 62: 213–225. https://doi.org/10.1016/j.jmgm.2015.10.004

Al-Sha'er MA, Mansi I, Khanfar M, Abudayyh A (2016) Discovery of new heat shock protein 90 inhibitors using virtual co-crystallized pharmacophore generation. Journal of Enzyme Inhibition and Medicinal Chemistry 31: 64–77. https://doi.org/10.1080/14756366.2016.1218485

Benincori T, Sannicoló F (1988) New access to 2-(arylazo)-, 2-(arylhydrazo)-, and 2-aminoindoles, -benzofurans, and –thianaphthenes. The Journal of Organic Chemistry 53: 1309–1312. https://doi.org/10.1021/jo00241a035

Biovia Software (2016) Biovia Software. https://www.3ds.com/products-services/biovia/disciplines/molecular-modeling-and-simulation

Boyd AE (1988) Sulfonylurea receptors, ion channels, and fruit flies. Diabetes 37: 847–850. https://doi.org/10.2337/diab.37.7.847

Butler RN, Scott FL (1970) Versatile reactive intermediates: Hydrazidic halides, Chem. Ind., London, 1216–1221.

Cheng T, Li X, Li Y, Liu Z, Wang R (2009) Comparative assessment of scoring functions on a diverse test set. Journal of Chemical Information and Modeling 49: 1079–1093. https://doi.org/10.1021/ci9000053

Diller DJ, Merz Jr KM (2001) High throughput docking for library design and library prioritization. Proteins: Structure, Function, and Bioinformatics 43: 113–124. https://doi.org/10.1002/1097-0134(20010501)43:2<113::AID-PROT1023>3.0.CO;2-T

Drews J (2000) Drug discovery: A historical perspective. Science 287: 1960–1964. https://doi.org/10.1126/science.287.5460.1960

Guardia CDL, Stephens DE, Dang HT, Quijada M, Larionov OV, Lleonart R (2018) Activity of novel quinoline derivatives against dengue virus Serotype 2. Molecules 23: 672–683. https://doi.org/10.3390/molecules23030672

Habashneh AY, El-Abadelah MM, Zihlif MA, Imraish A, Taha MO (2014) Synthesis and antitumor activities of some new N1-(flavon-6-yl) amidrazone derivatives. Archiv der Pharmazie 347: 415–422. https://doi.org/10.1002/ardp.201300326

Ilakiyalakshmi M, Napoleon AA (2022) Review on recent development of quinoline for anticancer activities. Arabian Journal of Chemistry 15: 104168–104202. https://doi.org/10.1016/j.arabjc.2022.104168

Jain S, Chandra V, Kumar Jain P, Pathak K, Pathak D, Vaidya A (2019) Comprehensive review on current developments of quinoline-based anticancer agents. Arabian Journal of Chemistry 12: 4920–4946. https://doi.org/10.1016/j.arabjc.2016.10.009

Kalaria PN, Karad SC, Raval DK (2018) A review on diverse heterocyclic compounds as the privileged scaffolds in antimalarial drug discovery. European Journal of Medicinal Chemistry 158: 917–936. https://doi.org/10.1016/j.ejmech.2018.08.040

Kashem MA, Nelson RM, Yingling JD, Pullen SS, Prokopowicz AS, Jones JW, Wolak JP, Rogers GR, Morelock MM, Snow RJ, Homon CA, Jakes S (2007) Three mechanistically distinct kinase assays compared: Measurement of intrinsic ATPase activity identified the most comprehensive set of ITK inhibitors. Journal of Biomolecular Screening 12: 70–83. https://doi.org/10.1177/1087057106296047

Khamis MA, Gomaa W, Ahmed WF (2015) Machine learning in computational docking. Artificial Intelligence in Medicine 63: 135–152. https://doi.org/10.1016/j.artmed.2015.02.002

Kitchen DB, Decornez H, Furr JR, Bajorath J (2004) Docking and scoring in virtual screening for drug discovery: methods and applications. Nature Reviews Drug Discovery 3: 935–949. https://doi.org/10.1038/nrd1549

Meng XY, Zhang HX, Mezei M, Cui M (2011) Molecular docking: A powerful approach for structure-based drug discovery. Current Computer-Aided Drug Design 7: 146–157. https://doi.org/10.2174/157340911795677602

Paprocka R, Wiese-Szadkowska M, Kosmalski T, Frisch D, Ratajczak M, Modzelewska-Banachiewicz B, Studzińska R (2022) A review of the biological activity of amidrazone derivatives. Pharmaceuticals 15: 1219–1239. https://doi.org/10.3390/ph15101219

Persoone G, Baudo R, Cotman M, Blaise C, Thompson KCl, Moreira-Santos M, Vollat B, Törökne A, Han T (2009) Review on the acute Daphnia magna toxicity test – Evaluation of the sensitivity and the precision of assays performed with organisms from laboratory cultures or hatched from dormant eggs. Knowledge and Management of Aquatic Ecosystems 1: 393–422. https://doi.org/10.1051/kmae/2009012

Ranjbar-Karimi R, Poorfreidoni A (2018) Incorporation of fluorinated pyridine in the side chain of 4-aminoquinolines: Synthesis, characterization and antibacterial activity. Drug Research. 68: 17–22. https://doi.org/10.1055/s-0043-116674

Rao SN, Head MS, Kulkarni A, Lalonde M (2007) Validation studies of the site-directed docking program LibDock. Journal of Chemical Information and Modeling 47: 2159–2171. https://doi.org/10.1021/ci6004299

Sang-sup J, Hyeung-geun P (2009) Cinchona-based phase-transfer catalysts for asymmetric synthesis. Chemical Communication 46: 7090–7103. https://doi.org/10.1039/b914028j

Ulrich H (1968) The Chemistry of Imidoyl Halides, Plenum Press, New York, 174–192. https://doi.org/10.1007/978-1-4684-8947-7

Sheldrick GM (2015a) SHELXT-integrated space-group and crystal-structure determination. Acta Crystallographica A71: 3–8. https://doi.org/10.1107/S2053273314026370

Sheldrick GM (2015b) Crystal structure refinement with SHELXL. Acta Crystallographica C71: 3–8. https://doi.org/10.1107/S2053229614024218

Sheldrick GM (1996) (SADABS). University of Göttingen, Germany.

Verdonk ML, Mortenson PN, Hall RJ, Hartshorn MJ, Murray CW (2008) Protein-ligand docking against non-native protein conformers. Journal of Chemical Information and Modeling 48: 2214–2225. https://doi.org/10.1021/ci8002254

Warren GL, Andrews CW, Capelli AM, Clarke B, LaLonde J, Lambert MH, Lindvall M, Nevins N, Semus F, Senger S, Tedesco G, Wall ID, Woolven JM, Peishoff CE, Head MS (2006) A critical assessment of docking programs and scoring functions. Journal of Medicinal Chemistry 49: 5912–5931. https://doi.org/10.1021/jm050362n

Yao H-C, Resnick PJ (1962) Azo-hydrazone conversion. I. The Japp-Klingemann reaction. Journal of the American Chemical Society 84: 3514–3517. https://doi.org/10.1021/ja00877a018

Supplementary material 1

Docking, synthesis, and anticancer assessment of novel quinoline-amidrazone hybrids

Authors: Ahmad H. Abdullah, Ahmad K. Alarareh, Mahmoud A. Al-Sha'er, Almeqdad Y. Habashneh, Firas F. Awwadi, Sanaa K. Bardaweel

Data type: docx

Link: https://doi.org/10.3897/pharmacia.71.e117192.suppl1

Supplementary material 2

Scanned IR, 1H NMR and 13C NMR spectra of all new compounds

Authors: Ahmad H. Abdullah, Ahmad K. Alarareh, Mahmoud A. Al-Sha'er, Almeqdad Y. Habashneh, Firas F. Awwadi, Sanaa K. Bardaweel

Data type: docx

Link: https://doi.org/10.3897/pharmacia.71.e117192.suppl2